Microscopic model of dispersive-motion relaxation

M. Engelsberg and Ricardo E. de Souza
Departamento de Física, Universidade Federal de Pernambuco 50670-901 Recife, Pernambuco, Brazil

Hsu Chang
Toshiba America MRI, Incorporated, 280 Utah Avenue, South San Francisco, California 94080

(Received 14 December 1995; revised manuscript received 23 August 1996)

Dispersive motional relaxation of ^{19}F nuclei in the superionic conductor β-PbF_2, lightly doped with monovalent K^+ ions, is studied by nuclear magnetic resonance. A microscopic model of the spatially nonuniform motion of ^{19}F nuclei in this disordered system, correctly predicts a wide range of observations. The model predicts the form of the nonexponential decay of the magnetization in the rotating frame and its change when the doping level is varied, the scaling of the decays with temperature and rotating field for a given doping level, and the observed departures from simple relaxation theory. [S0163-1829(96)01446-4]

I. INTRODUCTION

Relaxation in disordered systems has attracted considerable interest in recent years mainly as a consequence of some universal features that appear to be associated with the phenomenon. Unlike homogeneous crystalline solids and simple liquids, motional relaxation in disordered solids and variety of supercooled liquids is frequently nonexponential. In many cases, which include glassy systems, amorphous polymers, and orientationally disordered crystals, relaxation processes have been found to exhibit stretched exponential behavior over a considerable range. Stretched exponential time dependence of the relaxation of form $\exp[-(t/\theta)^{\beta}]$ with $0 \leqslant \beta \leqslant 1$, introduced by Kohlrausch[1,2] to describe mechanical creep in glassy fibers, has been found to be at least as ubiquitous and probably even more so than purely exponential relaxation.[3] Even though recent dielectric measurements in glass-forming supercooled liquids[4,5] indicate that Kohlrausch relaxation only prevails at relatively low frequencies, or correspondingly long times, it was found to still provide a satisfactory description for more than two decades of variation in frequency.

Another characteristic feature often found in the relaxation of disordered systems is non-Arrhenius temperature dependence whereby correlation times in glass-forming systems, for example, exhibit an apparent activation energy which is not constant but rather increases at low temperatures.[4] Moreover these peculiarities in the relaxation are often accompanied by an anomaly in the specific heat.[5]

Although some of these effects can be qualitatively understood in a simplistic way by assuming an heuristic probability distribution of correlation times which leads to dispersive relaxation, this approach does not shed light on the microscopic origin of the processes nor on its more general aspects. Thus, microscopic models of dispersive relaxation in real systems seem quite attractive.

From the point of view of NMR measurements, the superionic conductor PbF_2,[7,8] doped with small amounts of KF constitutes a model system which displays dispersive relaxation of a type which appears to be amenable to microscopic modeling. The motion of fluorine spins which emerges from such a model is predicted to be very fast but highly localized around the dopant ions at low temperatures. At higher temperatures, an increasingly larger number of spins around the dopant ions become mobile on the NMR time scale until fast motion prevails throughout the system. It is interesting to notice that this picture is to some extent reminiscent of the conditions prevailing in the glass transformation range of supercooled liquids. According to mode coupling theory,[9–11] as the temperatures is lowered, translational degrees of freedom get frozen in until the particles get arrested in the cages formed by other neighboring particles and the motion becomes localized. From a theoretical point of view, a glass transition, defined as occurring at a temperature where a structural correlation time becomes infinite, has been predicted to take place via a nonlinear feedback mechanism of density fluctuations.

In Sec. II of this paper we present ^{19}F rotating frame nuclear spin-lattice relaxation (RFNSLR) measurements in the β phase of PbF_2 doped with small amounts of KF. In Sec. III a microscopic model of dispersive relaxation which satisfactorily accounts for the experimental results is presented. In Sec. IV generalizations of the model and their possible applicability to more general processes are discussed.

II. EXPERIMENTAL

The data presented here include temperature and rotating field dependences of spin-lattice relaxation rates and decays in the rotating frame in β-PbF_2, single crystals with two different concentrations of K^+. Sample A contained 0.054 mole % KF whereas the concentration of KF in sample B was 0.0088 mole %. The rotating magnetic fields strengths employed were 0.68, 1.3, 1.89, and 2.5 mT and a 1.498 T static magnetic field, corresponding to a 60 MHz Larmor frequency for fluorine was applied along [100].

Figure 1 shows a typical nonexponential decay of the ^{19}F magnetization in the rotating frame for a radio-frequency field of amplitude $B_1 = 0.68$ mT at $T = 198$ K in sample A. Even though a rotating frame spin-lattice relaxation time cannot be defined in the usual way from data such as those of Fig. 1, it is still useful to introduce a characteristic time T_{1r}.

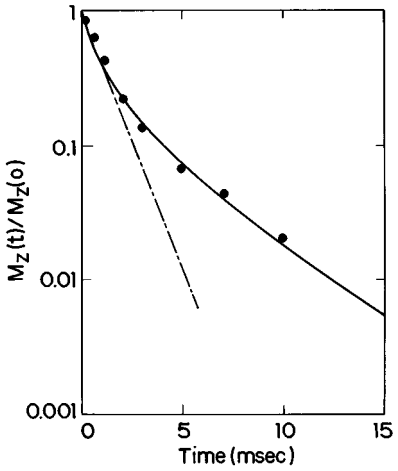

FIG. 1. Decay of the rotating frame magnetization in β-PbF_2:K^+ (sample A) for B_1=0.68 mT and T=198 K. The solid line was calculated at T=197 K with the two adjustable parameters used in all calculations: the fluoride vacancy prefactor $\tau_{v\infty}=8.5\times10^{-14}$ s and its activation energy E_v=0.185 eV/ion. The slope of the dashed line gives T_{1r}.

This permits a more concise description of the temperature and rotating field dependences of the relaxation rates also providing an adequate parameter to display the scaling of the decays. Although other choices are possible, it is convenient for the present case to define $\overline{T_{1r}}$ as the slope of a straight line fit of the initial decay, shown by the dashed line of Fig. 1. In order to avoid any ambiguity in comparing experimental and theoretical values of $\overline{T_{1r}}$ defined by this procedure, the points in the calculated decays joined by the dashed line of Fig. 1 were chosen at the same times as the ones employed for the experimental data.

Figure 2(a) shows the scaling behavior of the decays in sample A for various temperatures in the range 178 K $<T<$253 K and for all four rotating field amplitudes, when plotted as a function of reduced time $(t/T_{1r})^{0.63}$. Figure 2(b) shows similar decays for sample B exhibiting an analogous scaling when plotted as a function of $(t/T_{1r})^{0.70}$. In Fig. 3, the temperature dependence of T_{1r} for sample A is shown at two different values of B_1, whereas Fig. 4 shows the temperature dependence of T_{1r} in sample A and sample B at a single value of B_1.

Figure 5 shows the B_1 dependence of $\overline{T_{1r}}$ in sample A for a typical temperature T=208 K on the low-temperature side of the minima of Fig. 3.

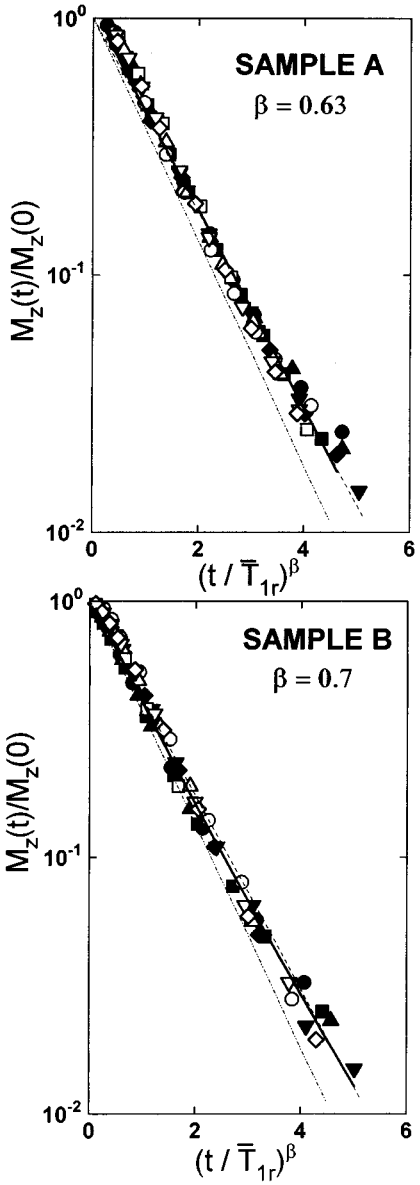

FIG. 2. Scaling plots of the decays of the magnetization in the rotating frame. The data, represented by different symbols, correspond to four values of B_1 and various temperatures in the range 178 K$<T<$253 K. The solid lines are theoretical fits whereas the dot-dashed lines represent stretched exponentials $\exp[-(t/T_{1r})^{\beta}]$ and the dashed lines represent the functions $\exp[-(t/0.8T_{1r})^{\beta}]$. (a) (top): scaling plot for sample A (0.054 mole % KF) as a function of reduced time $(t/T_{1r})^{\beta}$ with β=0.63. (b) (bottom): scaling plot for sample B (0.0088 mole % KF) as a function of reduced time $(t/T_{1r})^{\beta}$ with β=0.70.

III. MICROSCOPIC MODEL

The fluorite β phase of PbF_2 displays high anionic mobility reaching values typical of molten electrolytes at temperatures in the vicinity of 700 K. Moreover sufficient mobility to cause motional narrowing of the NMR line can be frozen in PbF_2, even at temperature as low as 200 K, by the addition of small amounts of monovalent[12] (K^+, Na^+) or trivalent ions[13] such as Eu^{3+}.

RFNSLR in pure PbF_2, at temperatures in the motionally narrowed line regime (330 K$<T<$520 K), appears to be well described, within the framework of the Bloembergen-Purcell-Pound (BPP) theory,[8,14] with a single fluorine jump rate. In contrast, for PbF_2:K^+ in a lower temperature range (160 K$<T<$400 K) but still corresponding to an equivalent motional regime, this description is no longer possible and dispersive relaxation with a distribution of jump rates appears to prevail. The experimental data of Fig. 3 resemble the theoretical predictions of the BPP theory with a single jump rate. However, the asymptotes on both sides of the minima have different slopes corresponding to apparent activation energies of 0.18 eV/ion on the high-temperature side and of 0.24 eV/ion on the low-temperature side. This may be

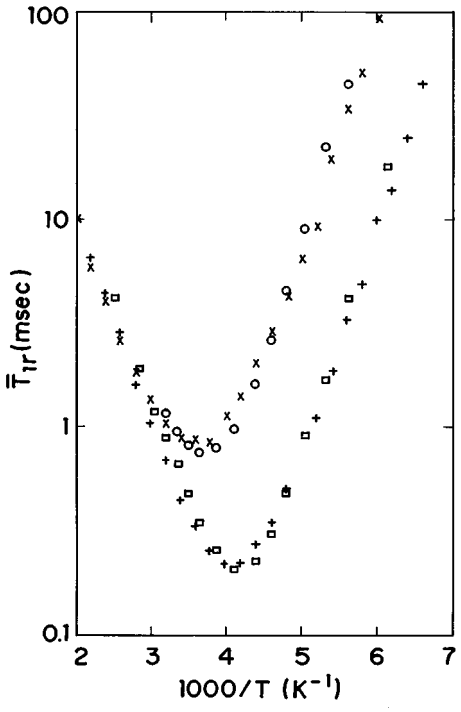

FIG. 3. Experimental (□) and theoretical (+) values of $\overline{T_{1r}}$ as a function of inverse temperature in sample A for B_1=0.68 mT. Theoretical values were obtained from the calculated decays using the same procedure shown by the dashed line of Fig. 1. Experimental (○) and theoretical (×) values of T_{1r} are also shown for B_1=2.5 mT. The slopes of the high-temperature asymptotes are 0.18 eV/ion whereas the low-temperature slopes are 0.24 eV/ion.

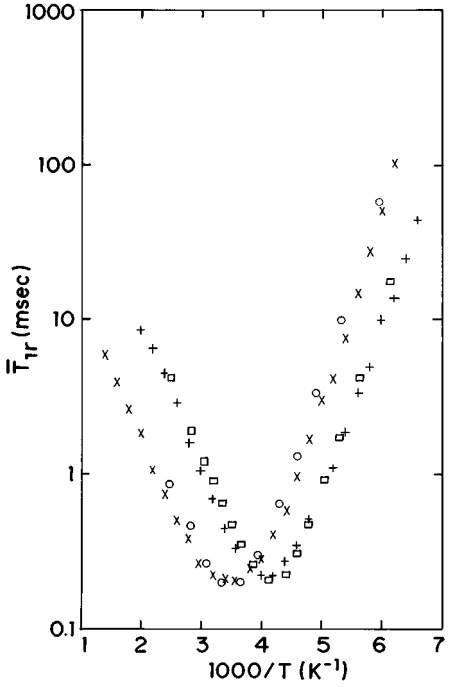

FIG. 4. Experimental (□) and theoretical (+) values of $\overline{T_{1r}}$ as a function of inverse temperature for B_1=0.68 mT in sample A. Experimental (○) and theoretical (×) values of T_{1r} are also shown for sample B.

interpreted as a non-Arrhenius behavior whereby the apparent activation energy becomes larger at low temperatures. Furthermore, the rotating field dependence shown in Fig. 5 yields $T_{1r} \propto B_1^{1.78}$ instead of a quadratic dependence.

NMR probes the relaxation of ^{19}F magnetic moments caused by mobile defects, which in the present case, are fluoride vacancies created by doping with monovalent alkaline ions which substitute[15] for divalent Pb^{2+}. For this type of disorder, the probability distribution of ^{19}F residence times τ_F can be modeled. Consider a single K^+ ion substituting for Pb^{2+} at the center of a sphere of radius R containing many fluorine nuclei and let r be the radial distance from the K^+ ion to a charge-compensating fluoride vacancy (F_v). Neglecting thermally induced defects in the temperature range of the experiment, the motion of fluorine nuclei can be assumed to be controlled by the spatially nonuniform probability distribution of fluoride vacancies. At low temperatures, and because of the Coulomb attraction binding K^+:F_v pairs, fluoride vacancies can be found with significant probability only for small values of r and fluorine motion only takes place in the vicinity of the doping ions. As the temperature increases and K^+:F_v pairs dissociate, a larger fraction of fluorines become mobile.

Denoting by $P(r,T)4\pi r^2 dr$ the probability of finding a fluoride vacancy within a spherical shell of radius between r and $r+dr$ and by $n_F 4\pi r^2 dr$ the number of fluorine nuclei within the same volume, the jump rate $1/\tau_F$ of a fluorine can be related to the jump rate $1/\tau_v$ of the vacancy by

$$1/\tau_F = [P(r,T)/n_F](1/\tau_v), \tag{1}$$

where $n_F = 3.778\times10^{22}$ cm^{-3} is the number of fluorines per unit volume. Furthermore, the fluoride vacancy motion within the sphere of radius R is assumed to be characterized by a single residence time with an *Arrhenius* dependence on temperature $\tau_v = \tau_{v\infty} \exp(E_v/kT)$.

For the proposed model of bound K^+:F_v pairs, the probability density $P(r,T)$ can be written as

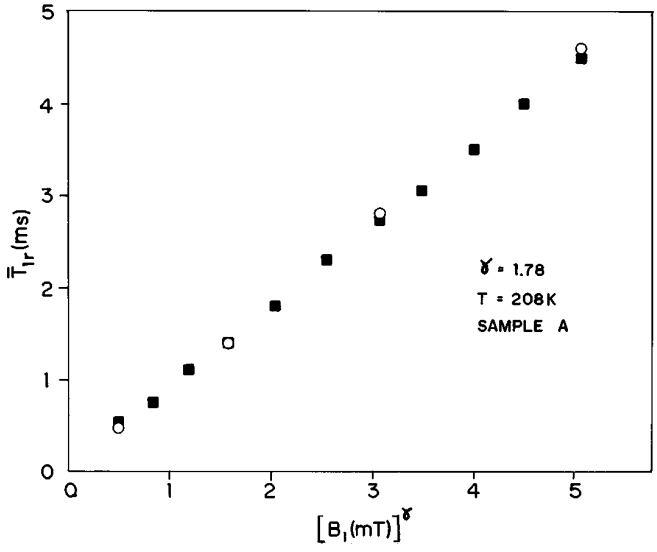

FIG. 5. $\overline{T_{1r}}$ as a function of $[B_1]^\gamma$ with γ=1.78 for sample A at T=208 K. Experimental values (○). Theoretical values (□).

$$P(r,T)=e^{-\Phi/kT}\Big/\int_{\Omega_a}e^{-\Phi/kT}d\Omega, \tag{2}$$

where $\Phi(r,T)$ is the potential energy of a fluoride vacancy at a distance r from a K^+ dopant and the integral extends over the volume Ω_a of spherical shell of influence, of outer radius R and inner radius b, surrounding a single K^+ dopant ion. Here b denotes the distance of closest approach between the fluoride vacancy and the K^+ ion.

The Coulomb attraction between the effective positive charge of a fluoride vacancy and the effective negative charge of a monovalent dopant ion is shielded by the ionic atmosphere. For the relatively low concentration of mobile defects in our samples, the net effect can be described by a simple Debye-Hückel[16,12] potential:

$$\Phi(r,T)=-[e^{\lambda b}/(1+\lambda b)](q^2/\epsilon r)e^{-\lambda r}, \tag{3}$$

where $\lambda=(6q^2/\epsilon kTR^3)^{1/2}$, q is the electronic charge, $\epsilon\cong 30$ is the large static dielectric constant of this superionic conductor,[17] R is the radius of a sphere containing a single dopant ion and $b=2.58$ Å is the distance of closest approach between the fluoride vacancy and the K^+ ion for the fluorite structure of β-PbF_2.

We further assume that each ^{19}F is relaxed directly by the fluctuating dipolar fields of neighboring mobile nuclei and that spin diffusion within a sphere of influence is slow compared with direct RFNSLR rates. For a ^{19}F spin at a distance r from the center of a sphere of influence, the rotating frame relaxation rate $1/T_{1r}$ predicted by the BPP theory is then given by[7]

$$1/T_{1r}=W\tau_F(r,T)/[1+4\omega_1^2\tau_F^2(r,T)], \tag{4}$$

where $\omega_1=\gamma_F B_1$, $\gamma_F=2.5166\times10^8\ T^{-1}\ s^{-1}$ denotes the gyromagnetic ratio of fluorine nuclei and $W=0.44\times10^{10}\ s^{-2}$ is approximately equal to the rigid lattice contribution to the second moment.

The time evolution of the magnetization parallel to $\vec{B}_1$ (along z), can be obtained from Eq. (4) by adding the contributions from all nuclei within the sphere of radius R containing a single dopant ion. However, given the disorder introduced by the random nature of the doping process, the radius R must be regarded as a random variable with a probability density $Q(R)$ to be determined. Since the substitution of sites by a given average concentration of dopants n_d can be expected to follow a binomial distribution, the probability that a sphere of radius R contains a single dopant ion can be calculated. Moreover if the sphere of radius R contains many Pb^{2+} sites with very small K^+ occupation probability, as in the present case, the binomial distribution becomes, to a very good approximation, a Poisson distribution. The probability that a sphere containing a single K^+ ion has a radius between R and $R+dR$, is then given by

$$Q(R)dR=4\pi R^2 n_d e^{-n_d(4/3)\pi R^3}dR\Big/\left(\int_b^\infty 4\pi\rho^2 n_d e^{-n_d(4/3)\pi\rho^3}d\rho\right). \tag{5}$$

The final time evolution of the overall rotating frame magnetization $M_z(t)$, averaged over the Poisson distribution $Q(R)$, can be obtained from Eqs. (1)–(5):

$$M_z(t)/M_z(0)=\int_b^\infty Q(R)\left\{[(3/4\pi)(R^3-b^3)^{-1}]\times\int_b^R e^{-t/T_{1r}}4\pi r^2 dr\right\}dR. \tag{6}$$

Various comparisons between the predictions of Eq. (6) and the experimental data are shown in Figs. 1–4 where the only two adjustable parameters were $\tau_{v\infty}=8.5\times10^{-14}$ s, corresponding to typical phonon frequencies, and $E_v=0.185$ eV/ion. The average number of dopants per unit volume n_d was obtained from the known concentrations of samples A and B and is better represented by an average radius $R=[3/(4\pi n_d)]^{1/3}$. For sample A, $R_A=30.4$ Å, while for sample B, $R_B=55.3$ Å.

Figure 1 shows a typical theoretical decay obtained by a numerical integration of Eq. (6) for $T=197$ K and $B_1=0.68$ mT in sample A. Figures 2(a) and 2(b) show theoretical decays with $\beta=0.63$ (sample A) and $\beta=0.70$ (sample B) which also exhibit the scaling behavior with respect to temperature and rotating field amplitude found experimentally. Figure 2(b) shows that the value of β which yields a straight line actually becomes closer to one as the degree of disorder is reduced. These results suggest that, for the range of time which is experimentally accessible, the experimental decays and the theoretical ones appear to be well described by a stretched exponential function $\exp[-(t/T_{1r})^\beta]$ shown as a straight line in Fig. 2. The agreement in the actual slopes could have been improved by defining T_{1r}, slightly differently, as the time corresponding to a decay of the magnetization to $1/e$ of its initial values. As suggested by the function $\exp[-(t/0.8T_{1r})^\beta]$ shown in Fig. 2, this would amount to a value of T_{1r} approximately 20% higher than the value resulting from the procedure of Fig. 1. It should be pointed out that the very short-time region of the experimental decays is affected by known transient effects[18] and a comparison with theory is therefore not possible there. It is also worth emphasizing that, unlike true stretched exponentials, the calculated decays have finite initial slopes and decay slower in this short-time region than the stretched exponential functions which fit the long-time regime (see Fig. 7 below).

Figures 3 and 4 show calculated values of $\overline{T_{1r}}$ where each point is obtained by first computing the decay from Eq. (6) and subsequently determining the time constant T_{1r} by the procedure outlined in Fig. 1 using points chosen at the same times as in the experimental decays. This procedure was also used to obtain the theoretical values of T_{1r} shown in Fig. 5

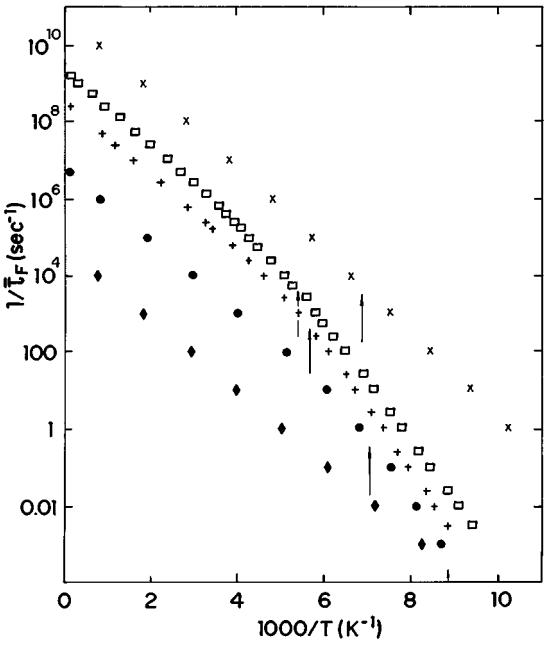

FIG. 6. Characteristic correlation rates $1/\overline{\tau_F}$, calculated from the value of B_1 at the minima of $\overline{T_{1r}}$, as a function of inverse temperature for (×) $R=10$ Å, (□) $R=30.4$ Å, (+) $R=55.3$ Å, (●) $R=210$ Å, and (♦) $R=1000$ Å. The arrows indicate the position of the peaks in the specific heat C_v.

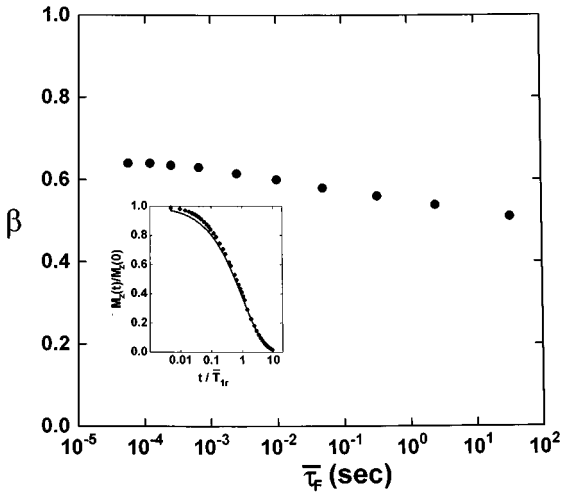

FIG. 7. The calculated stretching exponent β as a function of the characteristic correlation time $\overline{\tau_F}$ for sample A ($R=30.4$ Å). Inset: (●) theoretical decay as a function of the logarithm of reduced time for $R=30.4$ Å, $T=188$ K, and $T_{1r}=1.67$ ms. (−) Stretched exponential $\exp[-(t/T_{1r})^{\beta}]$ with $\beta=0.64$.

for various values of the rotating field strength at a fixed temperature.

The model yields the correct values of the exponent β for two different values of the concentration of dopants and accounts for the observed scaling with temperature and B_1 (Fig. 2). The model also quantitatively explains the shift in the temperature dependence of T_{1r} with concentration (Fig. 4) as well as the observed departures from simple relaxation theory (Figs. 3 and 5). Given the agreement between this wide range of data and the predictions of Eq. (6), using only the two standard parameters of relaxation theory, we conclude that a fairly complete microscopic description of dispersive motional relaxation caused by this type of mild disorder is possible.

IV. DISCUSSION

Although strictly speaking, the model described in Sec. III only applies to a slightly disordered ionic crystal which exhibits dispersive relaxation, the nature of the motion resulting from the breaking of K^+:F_v pairs simulates some of the characteristics which may prevail in real systems in the glass transformation region. It seems therefore worthwhile to explore the consequences of this qualitative analogy by surveying the predictions of the model for a wide range of variation of the external parameters.

From the value of temperature and rotating magnetic field strength B_{1m} at the minima of the theoretical curves in Fig. 3, one can calculate the temperature dependence of an average correlation time $\overline{\tau_F}=1/\gamma_F B_{1m}$, in a way similar to the procedure employed in dielectric relaxation measurements and well beyond the range of experimentally accessible T_{1r} values.

Figure 6 shows theoretical values of $1/\overline{\tau_F}$ for samples with various values of R as a function of inverse temperature. As in dielectric measurements in many glassy systems,[4] non-Arrhenius behavior with an apparent activation energy which increases at low temperatures is apparent in Fig. 6. Moreover the crossover from the high-temperature regime, with a single activation energy of 0.185 eV/ion, to the low-temperature region where a departure from Arrhenius behavior occurs, depends upon the concentration of defects. As the number of defects, represented in the model by K^+ ions increases, the crossover temperature also increases. For values of R smaller than 10 Å, the crossover temperature begins to decrease with an increasing number of defects.

Another aspect which deserves attention concerns the range of validity of the stretched exponential decay predicted by the model and whether a universal exponent β, independent of temperature and B_1 is actually predicted for a given concentration of defects. The inset of Fig. 7 shows a plot of the theoretical decay obtained from Eq. (6) at $T=188$ K and $\overline{R_A}=30.4$ Å together with a stretched exponential function with $\beta=0.64$. It is apparent that for approximately two decades in time the agreement is very good, as it is in this long-time region the agreement between the experimental data and the calculated decays shown in Fig. 2. For short times the calculated decay begins to deviate from a stretched exponential. This behavior is also observed in the imaginary part $\mathcal{E}''$ of the dielectric susceptibility in various glass formers[4,6] where, after approximately two decades of frequency increase from the maximum of $\mathcal{E}''$, the decays begin to deviate from the prediction of a stretched exponential, but appearing instead to become slower in the frequency domain. We conclude that the present model predicts a stretched exponential decay for approximately the same range of long times or low frequencies where it appears to be valid in real systems.

Although Figs. 2(a) and 2(b) suggest a universal exponent β independent of temperature and B_1, a more stringent test

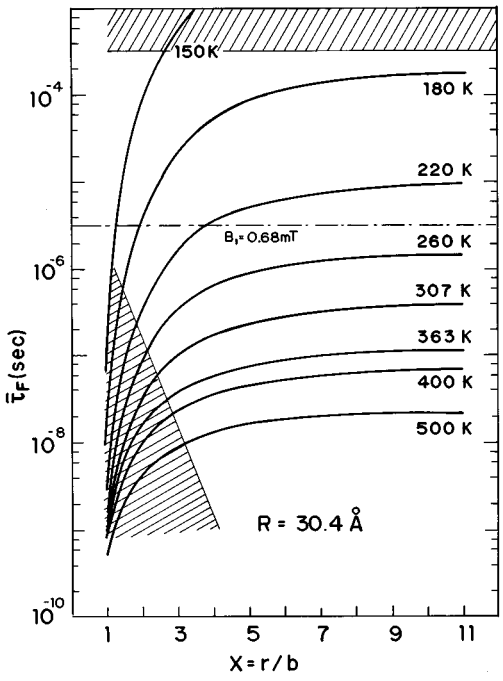

FIG. 8. Correlation times τ_F within a sphere of influence of radius $R=30.4$ Å as a function of temperature and radial distance. The horizontal dashed line corresponds to the condition $2\gamma_F B_1 \tau_F = 1$ for $B_1 = 0.68$ mT. The shaded areas correspond to approximate regions where the negligible spin diffusion condition is violated.

involving a much wider range of correlation times appears to be desirable. Figure 7 shows the variation of the stretching exponent in samples A for decays spanning seven decades in the correlation time. The values of β were found to be well defined on the low-temperature side of the T_{1r} minima and completely independent of B_1. Close to a minimum and on the high-temperature side, the calculated decays could no longer be represented by a stretched exponential.

Confirming the results of Fig. 2 in the accessible range of RFNSLR measurements, the calculated stretching exponents of Fig. 7 obtained from the present model, can be seen to exhibit a negligible variation in this range. However when large changes in the correlation time are involved, a small decrease with decreasing temperature becomes apparent.

The model also enables one to readily calculate the contribution to the specific heat C_v resulting from the dissociation process of K^+F_v pairs. From Eqs. (2) and (3), the energy

$$\overline{E_\Phi} = \int_b^R \Phi e^{-\Phi/kT} 4\pi r^2 dr \Big/ \int_b^R e^{-\Phi/kT} 4\pi r^2 dr, \quad (7)$$

can be calculated and the contribution to the specific heat at constant volume $C_v = (\partial \overline{E_\Phi}/\partial T)_v$, computed numerically. The result exhibits peaks in C_v at temperatures which depend upon the concentration of defects as indicated by the arrows in Fig. 6. For sample A, with $R=30.4$ Å, a peak value of 48 cal/K mole (K^+) with a half width of 50 K was obtained. Thus, the model predicts a thermal anomaly whose origin resides in a change from localized motion to one in which a large fraction of atoms become mobile.

Given the central role played in the present model by motion spatially localized around defects and the dissociation of K^+:F_v pairs, it is interesting to display directly the spatial and temperature dependence of the correlation time $\tau_F(r,T)$ given by Eqs. (1)–(3). Figure 8 shows calculated values of $\tau_F(r,T)$ for $b \leq r \leq R$, where $b=2.58$ Å denotes the distance of closest approach and $R=30.4$ Å is the radius of the sphere of influence characteristic of sample A. The condition $2\omega_1 \tau_F(r,T)=1$ for a minimum of T_{1r} of Eq. (4), is represented by the horizontal line for one of the experimental values of $B_1 = \omega_1/\gamma_F = 0.68$ mT. On the NMR time scale defined by a characteristic time $W^{-1/2} \sim 10^{-5}$ s, Fig. 8 clearly depicts the localization of motion which takes place at low temperatures and is the origin of dispersive relaxation in the present model. At these low temperatures only the first shells of fluorine nuclei around the dopant ion can be seen to remain mobile but with a motion which may be quite fast on the NMR time scale.

The calculated values of Fig. 8 also permit us to establish limits for the validity of the negligible spin-diffusion approximation implicit in Eq. (4). Denoting by $\delta t_{\rm dif}$ the spin-diffusion time for a distance δr, the condition of negligible spin diffusion would require $\delta t_{\rm dif} > \delta T_{1r}$, where δT_{1r} represents the corresponding variation in T_{1r} [Eq. (4)] at a given temperature and radial distance r. For $\sqrt{\delta t_{\rm dif}} = \delta r/\sqrt{D}$, where D denotes the spin-diffusion constant,[19] and $\delta r = a = (2/\sqrt{3})b$, where a is the nearest-neighbor fluorine-fluorine distance, one obtains the following conditions for negligible spin diffusion at $x=r/b$:

$$d\tau_F/dx < Wb^2/2\sqrt{3}\omega_1^2 D, \quad \text{for } 2\omega_1\tau_F \gg 1, \quad (8)$$

$$d\tau_F/dx < 2Wb^2\tau_F^2/\sqrt{3}D, \quad \text{for } 2\omega_1\tau_F \ll 1. \quad (9)$$

The shaded areas in Fig. 8 represent approximate regions where, either Eqs. (8) or (9), are violated for $D \sim 10^{-13}$ cm^2/s. It is clear from Fig. 8 that, on the low-temperature side of the minimum and for temperatures not lower than approximately 165 K, the condition for direct relaxation with negligible spin diffusion is satisfied approximately for all fluorines beyond the first shell around the impurity. This temperature region, as well as the corresponding temperature regions for other values of B_1, exhibit stretched exponential behavior, over a considerable range, with a stretching exponent accurately predicted by the model, as shown in Fig. 2.

As the temperature is raised above 220 K in Fig. 8, an increasingly larger number of fluorine shells become affected by spin diffusion which is expected to influence initially the long-time behavior of the decays. The suppression of magnetization gradients by spin diffusion tends to establish a uniform spin temperature and is expected to lead, progressively, to exponential decays. This is actually observed experimentally at the minima and on their high-temperature side. Nevertheless the experimental values of T_{1r} in this region, as defined by the procedure outlined in Fig. 1, are still in agreement with the predictions of the model.

V. CONCLUSIONS

The microscopic model of dispersive motional relaxation introduced in Sec. III quantitatively explains a wide range of

RFNSLR data in the superionic conductor PbF_2:K^+ with only two standard parameters. It yields the correct decays of the magnetization in the rotating frame for two different values of the concentration of dopants. The model also accounts for the observed scaling with temperature and B_1 of the decays, it quantitatively explains the shift in the temperature dependence of T_{1r} as the concentration of dopants is varied and the departures from simple relaxation theory. Thus, the non-Arrhenius behavior and the rotating field dependence of $\overline{T_{1r}}$ are also explained. Moreover, given the portrait of the motion emerging from the model, which mimics some of the characteristics believed to prevail in the glass transformation region of real systems, it also suggests how other predictions such as stretched exponential relaxation over a considerable range, a characteristic non-Arrhenius behavior, and a thermal anomaly, may originate in the peculiar dispersive nature of the motion.

ACKNOWLEDGMENTS

We wish to thank Professor Irving J. Lowe for hospitality and fruitful discussions and Professor J. J. Fontanella for making available the crystals used in this work. We also thank CNPq (Brazil) for support (M.E. and R.E.S.).

[1] R. Kohlrausch, Pogg. Ann. Phys. **91**, 179 (1854).
[2] G. Williams and D. C. Watts, Trans. Faraday. Soc. **66**, 80 (1970); K. S. Cole and R. H. Cole, J. Chem. Phys. **9**, 341 (1941).
[3] R. Böhmer, K. L. Ngai, C. A. Angell, and D. J. Plazek, J. Chem. Phys. **99**, 4201 (1993).
[4] Paul K. Dixon, Lei Wu, Sidney R. Nagel, Bruce D. Williams, and John P. Carini, Phys. Rev. Lett. **65**, 1108 (1990).
[5] K. O. Davies and G. O. Jones, Adv. Phys. **2**, 370 (1953).
[6] Diandra L. Leslie-Pelecky and Norman O. Birge, Phys. Rev. Lett. **72**, 1232 (1994).
[7] T. Y. Hwang, M. Engelsberg, and I. J. Lowe, Chem. Phys. Lett. **30**, 303 (1975).
[8] J. B. Boyce, J. C. Mikkelsen, Jr., and M. O'Keefe, Solid State Commun. **21**, 955 (1977), and references therein.
[9] E. Leutheuser, Phys. Rev. A **29**, 2765 (1984).
[10] U. Bengtzelius, W. Götze, and A. Sjölander, J. Phys. C **17**, 5915 (1984).
[11] W. Götze and L. Sjörgen, J. Phys. Condens. Matter **1**, 4183 (1989).
[12] Hsu Chang, M. Engelsberg, and I. J. Lowe, Solid State Ionics **5**, 609 (1981); Hsu Chang, Ph.D. thesis, University of Pittsburgh, 1981.
[13] Andries Meijerink and John C. Wright, Phys. Rev. B **447**, 2970 (1993).
[14] N. Bloembergen, E. M. Purcell, and R. V. Pound, Phys. Rev. **73**, 679 (1948).
[15] G. C. Liang and A. V. Joshi, J. Electrochem. Soc. **122**, 446 (1975).
[16] P. W. Debye and E. Hückel, Phys. Z. Sowjetunion **24**, 185 (1923); for a recent review of Debye-Hückel theory and criticality, see Michael E. Fisher, J. Stat. Phys. **75**, 1 (1994); Y. Levin, X. J. Li, and Michael E. Fisher, Phys. Rev. Lett. **73**, 2716 (1994).
[17] G. A. Samara, Phys. Rev. **13**, 4529 (1978).
[18] R. L. Strombotne and E. L. Hahn, Phys. Rev. **133**, A1616 (1964).
[19] A. Abragam, *Principles of Nuclear Magnetism* (Oxford University Press, Oxford, 1961), Chap. V.